The current issue and full text archive of this journal is available at
www.emeraldinsight.com/0961-5539.htm

Finite element modelling of electro-osmotic flows on unstructured meshes

A.K. Arnold, P. Nithiarasu and P.G. Tucker
School of Engineering, University of Wales Swansea, Swansea, UK

Received 18 April 2006
Revised 19 September 2006
Accepted 30 September 2006

Abstract

Purpose – This paper seeks to numerically model electro-osmotic flow (EOF) through microchannels using a finite element-based unstructured mesh solution methodology.

Design/methodology/approach – The finite element method (FEM) combined with the characteristic-based split (CBS) algorithm is used to solve the coupled Navier-Stokes equations in order to simulate EOFs. The Laplace and Poisson-Boltzmann equations are solved explicitly a priori to the solution of the fluid dynamic equations. The external electric field and internal potential values are then used to construct the source terms of the fluid dynamics equations.

Findings – Proposed methodology works excellently on unstructured meshes for both two- and three-dimensional flow problems. The results obtained for benchmark channel flow problems show an excellent agreement with analytical and experimental data.

Originality/value – The idea of using the FEM and the CBS algorithm to solve the governing equations of EOFs is proposed. This particular method of solving these equations is unprecedented. In addition to benchmark examples, a problem of practical importance is also solved in this paper.

Keywords Flow, Finite element analysis, Meshes

Paper type Research paper

1. Introduction

The number of transistors packed on to each integrated chip is expected to double approximately every two years according to Moore's (1965) law. Intel (2006) have recently announced a new chip with one billion transistors packed on to it, which is roughly twice the number of transistors than the previous version had. It follows that the heat produced on the chips will also double. Therefore, an efficient and reliable cooling system to remove heat from hot spots on the chips is a necessity.

There are many cooling methods currently employed to remove heat in electronic devices. In laptop computers, for example, these include developing cooling devices consisting of particular arrangements of fans (Khuan and Ratnam, 2006). Heat pipes are also commonly employed to cool electronic equipment (Jon Zuo *et al.*, 2001), as are droplet impingement methods (Amon *et al.*, 2005). Even though these methods succeed in lowering the temperature of a CPU, they are bulky and occupy a considerable amount of space.

The limit for using solely air for cooling systems in microelectronics is fast approaching (Heydari and Gektin, 2004). Some even believe that this limit has been reached (Johnson *et al.*, 2002). As devices become smaller and the number of components packed on to each chip increases year by year, the demand for better cooling systems is increasing.

International Journal of Numerical Methods for Heat & Fluid Flow
Vol. 18 No. 1, 2008
pp. 67-82

0961-5539
DOI 10.1108/09615530810839750

Pumped liquid cooling systems show great potential as alternative cooling methods at microscale. This is partly due to the fact that liquids are better transport media than air and have larger heat capacity and higher thermal conductivity than air.

There are two main categories of micropumps used for electronics cooling: membrane displacement pumps and field induced pumps. Pumps such as piezoelectric, electrostatic and electromagnetic are classed as membrane displacement pumps where as field induced pumps include: electro-osmotic, electrohydrodynamic and magnetohydrodynamic pumps. Amongst the various pumps mentioned above, piezoelectric and electro-osmotic pumps are the only pumps capable of producing pressures greater than 1 atm (Zeng *et al.*, 2001).

Compared to piezoelectric and other mechanical micropumps, electro-osmotic pumps are reliable as they contain no moving parts, are relatively easy to manufacture, as they contain no valves which would complicate the fabrication and sealing of the pump and have the added advantage of being silent.

The principles of electro-osmosis were originally discovered by Reuss in 1809 (Probstein, 1989). Since, then there has been growing interest in this area due to its applications in soil mechanics (Lewis and Humpheson, 1973; Lewis and Garner, 1972). However, most of the recent research in this area concentrates on using this principle in microscale applications.

Most surfaces acquire a finite charge when in contact with aqueous solution. The charged surface then attracts counterions while repelling the coions. This process creates a high concentration of counterions close to the charged surface. The layer close to the charged surface, which contains more counterions than coions, is called electric double layer (EDL). When such an aqueous electrolytic solution is subjected to an external electric field, applied parallel to the charged surface, mass migration of the counterions inside the EDL takes place towards the appropriate electrode. This mass migration of the charged ions drags along the nearby ions with them (Hunter, 1981). This creates a flat velocity profile. The whole process is referred to as electro-osmotic flow (EOF).

The latest research on electro-osmotic micropumps concentrates on finding appropriate material structure to increase the charged surface area whilst still maintaining a viable flow path. It appears, from the simple analytical theories, that the flow area is inversely proportional to the pumping efficiency. The smaller the passage size the better the efficiency. By fabricating an electro-osmotic micropump out of fused silica capillaries packed with silica particles (Zeng *et al.*, 2001) have managed to produce pressures of 20 atm at 2 kV, using multiple channels. There are numerous other experimental studies available in this area including references (Sim *et al.*, 2003; Johnson *et al.*, 2002; Zhou *et al.*, 2004; Jiang *et al.*, 2002; Dutta *et al.*, 2001).

EOF has also been studied by various theoretical groups such as Burgreen and Nakache (1964) and Rice and Whitehead (1965) who both produced analytical studies of electro-osmosis through capillaries. Their work has been extended by many others, including Kang *et al.* (2002) and Fu *et al.* (2003). There are several numerical studies on EOF available in the literature. The finite difference method (FDM) seems to be the most popular method. This method is also used by Yang *et al.* (2001a) to solve the Nernst-Planck equations, concentrating on fluid in the entry region between two parallel plates. They concluded that the EDL was thinner in the entrance region, but the ionic charge distribution in the fluid followed the Boltzmann distribution in the

region of the channel where flow was fully developed. This was further confirmed by a study carried out by Chen *et al.* (2004), who found that along the axial flow direction, when the flow is fully developed, the electric potential and net charge density are constant. Thus, the Poisson-Boltzmann equation is sufficient to describe the electro-osmotic (internal) potential if flow is fully developed. The FDM is also used by both Hu *et al.* (1999) and Yang *et al.* (2001b) to solve the Poisson-Boltzmann and Laplace equation coupled with the Navier-Stokes equations using a primitive variable approach.

In Patankar and Hu (1998), a semi-implicit finite volume method is used to solve the governing equations. They concentrate on controlling the shape of the velocity profile and simulate flow through 3D geometries, which is an area where only a limited number of studies are available.

The studies using the finite element method (FEM) are both rare and relatively new in the field of EOF. For example, Bianchi *et al.* (1998) investigate EOF and pressure driven flows in a T-junction. They use a two-step method, in which the electro-osmotic potential and externally applied fields are solved first and then their effect is included in the Navier-Stokes equations as a source term. As pointed out by Borges *et al.* (2002), who also used FEM as a numerical method, FEM offers flexibility to solve EOF in complicated domains.

The experimental work carried out in the area of EOF-based electronic cooling is promising and offers a potential solution to cooling problems (Zeng *et al.*, 2001; Dutta *et al.*, 2001). Considering the potential of electro-osmotic pumps to cool microprocessor chips, it is evidently beneficial to thoroughly investigate this procedure. It appears that the EOF-based cooling systems developed in the past are rarely guided by numerical studies. This is partly due to the lack of appropriate numerical algorithms to solve complicated problems on unstructured meshes. Thus, the present study concentrates on developing, testing and using an unstructured-based EOF solver for general applications.

The solution method proposed in the present work includes the explicit discretisation of the Poisson-Boltzmann and Laplace equations using a pseudo time term. This is similar to the approach introduced by Yang *et al.* (2001b). However, in the proposed algorithm, the incompressible Navier-Stokes equations are also solved using a fully explicit time discretisation via an artificial compressibility. The fully explicit characteristic-based split (CBS) algorithm has been widely used in various incompressible flow applications in the past (Nithiarasu, 2003; Nithiarasu *et al.*, 2004). However, the present work is the first attempt to use fully explicit CBS to solve EOF. The proposed algorithm includes the solution to the Poisson-Boltzmann and Laplace equations independent of Navier-Stokes equations followed by the solution to the modified Navier-Stokes equations.

2. Governing equations of microchannel electro-osmotic flows

The model used here to simulate electro-osmotically induced fluid flow in a microchannel, is based on the Navier-Stokes equations. The extra force term acting very close to the channel walls is added to the momentum equation as a source term, resulting in a modified form of the momentum equation. As mentioned before, the aqueous electrolyte must be subjected to an external electric field to drive the flow. The electric field is modelled using the Laplace equation, i.e.:

$$\frac{\partial^2 \phi}{\partial x_i^2} = 0. \tag{1}$$

The aqueous electrolyte contains both positive and negative ions. The Poisson equation can be used to describe the electrostatic potential of the surface (Hunter, 1981). The Boltzmann equation can be used to describe the two different types of ions of equal but opposite charge (Yang *et al.*, 2001b). As the flow is generally fully developed and has a small Peclet number, the ions inside the fluid are assumed to follow a Boltzmann distribution. The net charge density of the fluid can be substituted into the Poisson equation to form the Poisson-Boltzmann equation. The following non-linear Poisson-Boltzmann equation is then solved to obtain the internal potential:

$$\frac{\partial^2 \psi}{\partial x_i^2} = -\frac{2n_0 ze}{\varepsilon \varepsilon_0} \sinh\left(\frac{ze\psi}{k_b T}\right). \tag{2}$$

where ψ, internal potential; n_0, bulk concentration; ε, dielectric constant; ε_0, permittivity of a vacuum $= 8.85 \times 10^{-12}$ C/Vm; z, valence of the ion; e, the fundamental charge $= 1.602 \times 10^{-19}$; k_b, Boltzmann constant $= 1.308 \times 10^{-23}$ and T, absolute temperature.

At microscale level, the extra forces acting within the EDL have to be taken into account (Karniadakis *et al.*, 2005). Therefore, EOF through a microchannel is modelled using the modified Navier-Stokes equations for incompressible flow, which incorporate the electrokinetic effects. They are given as:

The continuity equation:

$$\frac{1}{\beta^2}\frac{\partial p}{\partial t} + \frac{\partial u_i}{\partial x_i} = 0, \tag{3}$$

where β is an artificial compressibility parameter.

The modified momentum equation:

$$\frac{\partial U_i}{\partial t} + \frac{\partial (u_j U_i)}{\partial x_j} = -\frac{\partial p}{\partial x_i} + \frac{\partial \tau_{ij}}{\partial x_j} - \rho_E \left(\frac{\partial (\psi + \phi)}{\partial x_i}\right), \tag{4}$$

and where τ_{ij} are the deviatoric stress components given by:

$$\tau_{ij} = \mu\left(\frac{\partial u_i}{\partial x_j} + \frac{\partial u_j}{\partial x_i} - \frac{2}{3}\frac{\partial u_k}{\partial x_k}\delta_{ij}\right). \tag{5}$$

Here:

$$\delta_{ij} = \begin{cases} 1 & i = j \\ 0 & i \neq j \end{cases},$$

where $i, j, k = 1, 2, 3$ (k is independent of i and j), $\rho_E(\nabla(\psi + \phi)$ is the source term and β is an artificial compressibility parameter. In the source term of equation (4), ρ_E is the charge density, given by:

$$\rho_E = -2n_0 ze \sinh\left(\frac{ze\psi}{k_b T}\right). \tag{6}$$

The governing equations (1)-(4) may be non-dimensionalised as discussed below. The equations are completed by appropriate initial and boundary conditions.

3. Non-dimensional scales

The non-dimensional forms of the above equations can be obtained by using the following scales:

$$\begin{gathered} u_i^* = \frac{u_i}{u_{\text{ref}}}; \quad \beta^* = \frac{\beta}{u_{\text{ref}}}; \quad x_i^* = \frac{x_i}{L_{\text{ref}}}; \quad t^* = \frac{tu_{\text{ref}}}{\text{L}_{\text{ref}}}; \quad p^* = \frac{p - p_{\text{ref}}}{\rho_{\text{ref}} u_{\text{ref}}^2}; \\ \psi^* = \left(\frac{ze\psi}{k_b T}\right); \quad \phi^* \left(\frac{ze\phi}{k_b T}\right); \quad u_{\text{ref}} = \frac{E_x \varepsilon \varepsilon_0 \zeta}{\mu}; \quad L_{\text{ref}} = W, \end{gathered} \tag{7}$$

where W, width of the microchannel, μ, dynamic viscosity of the liquid, ζ, zeta potential, E_x, applied electric field per unit length and subscript ref represents a reference quantity.

Substitution of above scales give following non-dimensional forms of the governing equations:

The Laplace equation:

$$\frac{\partial^2 \phi^*}{\partial x_i^{*2}} = 0. \tag{8}$$

Poisson-Boltzmann equation:

$$\frac{\partial^2 \psi^*}{\partial x_i^{*2}} = ka^2 \sinh(\psi^*), \tag{9}$$

where:

$$ka = W\left(\frac{2n_0 z^2 e^2}{\varepsilon \varepsilon_0 k_b T}\right)^{1/2}. \tag{10}$$

Continuity equation:

$$\frac{1}{\beta^{*2}} \frac{\partial p^*}{\partial t^*} + \frac{\partial U_i^*}{\partial x_i^*} = 0. \tag{11}$$

Momentum equation:

$$\frac{\partial U_i^*}{\partial t^*} + \frac{\partial \left(u_j^* U_i^*\right)}{\partial x_j^*} = -\frac{\partial p^*}{\partial x_i^*} + \frac{1}{Re} \frac{\partial \tau_{ij}^*}{\partial x_j^*} + G_x \sinh \psi^* (\nabla(\psi^* + \phi^*)). \tag{12}$$

where:

$$G_x = \frac{2n_0 k_b T \rho_{\text{ref}} L_{\text{ref}}^2}{\mu^2 Re^2}; \quad Re = \frac{\rho_{\text{ref}} u_{\text{ref}} L_{\text{ref}}}{\mu} = \rho_{\text{ref}} \left(\frac{E_x \varepsilon \varepsilon_0 \zeta}{\mu} \right) \left(\frac{L_{\text{ref}}}{\mu} \right), \tag{13}$$

and:

$$\tau_{ij}^* = \left(\frac{\partial u_i^*}{\partial x_j^*} + \frac{\partial u_j^*}{\partial x_i^*} - \frac{2}{3} \frac{\partial u_k^*}{\partial x_k^*} \delta_{ij} \right). \tag{14}$$

From here onwards, the asterisks will be dropped for the sake of simplicity.

4. Numerical solution strategy

The partial differential equations which govern fluid flow in the microchannels have to be solved numerically. However, the Laplace equation (8) and the Poisson-Boltzmann equation (9) can be decoupled from the Navier-Stokes equations and solved separately (Hu *et al.*, 1999).

To begin the calculation, both the Laplace and Poisson-Boltzmann equations are solved explicitly. This consists of adding a pseudo time term – which becomes negligible when a steady state solution is reached. This is similar to the method used by Yang *et al.* (2001b).

The pseudo time dependent Laplace equation:

$$\frac{\partial \phi}{\partial t} + \nabla^2 \phi = 0, \tag{15}$$

is temporally discretized using a forward difference approach and then the standard Galerkin FEM is used.

The Poisson-Boltzmann equation is solved in a similar manner. The solutions to the Laplace equation and the Poisson-Boltzmann equation are then used to calculate the source term of the momentum equation.

The CBS algorithm is used in the present study to solve the modified incompressible Navier-Stokes equations. The instability in the scheme created by the pressure term in the momentum equation is overcome by introducing the split. The split method, combined with a characteristic Galerkin approximation, was first used to solve the Navier-Stokes equations by Zienkiewicz and Codina (1995).

This method originates from the simple characteristic method which is an explicit scheme and is based on a Taylor expansion (Löhner *et al.*, 1984). The CBS scheme involves splitting the solution to the Navier-Stokes equations into three steps.

These steps are summarised as:

(1) solve the momentum equation without pressure (this is done by introducing an intermediate velocity field);

(2) solve for pressure; and

(3) correct the momentum.

4.1 CBS algorithm

The semi-discrete form of Step 1 is:

$$\begin{aligned}\Delta U^{\dagger} &= U_i^{\dagger} - U_i^n \\ &= \Delta t\left[-\frac{\partial(U_i u_j)}{\partial x_j} + \frac{1}{Re}\,\frac{\partial \tau_{ij}}{\partial x_j} - G_x \sinh\psi \frac{\partial(\psi+\phi)}{\partial x_i}\right]^n \\ &\quad + \frac{\Delta t^2}{2}\, u_k \frac{\partial}{\partial x_k}\left[\frac{\partial(U_i u_j)}{\partial x_j} - \frac{1}{Re}\left(\frac{\partial \tau_{ij}}{\partial x_j}\right) + G_x \sinh\psi \frac{\partial(\psi+\phi)}{\partial x_i}\right]^n,\end{aligned} \tag{16}$$

where $U_i^{\dagger}$ = intermediate momentum field, $u_i^n = u_i(t_n)$ and $\Delta t = t^{n+1} - t^n$.

The pressure is solved at Step 2 as:

$$\left(\frac{1}{\beta^2}\right)^n (p^{n+1} - p^n) = -\Delta t \frac{\partial U_i^{n+\theta_1}}{\partial x_i}. \tag{17}$$

The momentum correction Step 3 is given as:

$$\frac{U_i^{n+1} - U_i^{\dagger}}{\Delta t} = -\frac{\partial P^{n+\theta_2}}{\partial x_i} + \frac{\Delta t}{2}\, u_k \frac{\partial}{\partial x_k}\left(\frac{\partial p^n}{\partial x_i}\right)^n. \tag{18}$$

Substitution of U^{n+1} from equations (18) into (17) gives:

$$\begin{aligned}\left(\frac{1}{\beta^2}\right)^n (p^{n+1} - p^n) &= -\Delta t\left[\theta_1 \frac{\partial U_i^{\dagger}}{\partial x_i} + (1-\theta_1)\frac{\partial U_i^n}{\partial x_i}\right] \\ &\quad + \Delta t \theta_1 \frac{\partial}{\partial x_i}\left[\theta_2 \frac{\partial p^{n+1}}{\partial x_i} + (1-\theta_2)\frac{\partial p^n}{\partial x_i} - \frac{\Delta t}{2}\, u_k \frac{\partial}{\partial x_k}\left(\frac{\partial p^n}{\partial x_i}\right)\right],\end{aligned} \tag{19}$$

where $0.5 < \theta_1 < 1.0$ and $\theta_2 = 0$ for a fully explicit scheme. More details on the fully explicit algorithm and the selection of artificial compressibility parameter, β, readers are referred to references: Nithiarasu (2003), Nithiarasu *et al.* (2004), Lewis *et al.* (2004) and Zienkiewicz *et al.* (2005).

The resulting equations are then spatially discretized using a Galerkin finite element procedure (Zienkiewicz *et al.*, 2005). The spatial discretisations are carried out as follows:

$$U_i^{\dagger} = \sum_{a=1}^{m} N^a \bar{U}_i^{\dagger a}; \quad U_i = \sum_{a=1}^{m} N^a \bar{U}_i^a; \quad p = \sum_{a=1}^{m} N^a \bar{p}^a. \tag{20}$$

The overline indicates a nodal quantity, m is the number of nodes in the element in question and a represents a particular node. Once these equations have been spatially discretised, they are weighted by the shape functions and then integrated over the domain.

The final matrix form of the first step may be written, without third and higher order terms, as:

$$\mathbf{M}\Delta\bar{U}_i^{\dagger} = \Delta t[-\mathbf{C}\bar{\mathbf{U}}_\mathbf{i} + \mathbf{K}_{\pi i} + \mathbf{F}_i] + \frac{\Delta t^2}{2}[\mathbf{K}_\mathbf{u}\bar{\mathbf{U}}_\mathbf{i}] + \mathbf{f}_{\tau\mathbf{i}}. \tag{21}$$

In the above equation the boundary terms from the extra second order terms (stabilization terms) are neglected. The matrices are given as:

$$\mathbf{M} \equiv \int_\Omega \mathbf{N}^T\mathbf{N}\mathrm{d}\Omega; \quad \mathbf{C} \equiv \int_\Omega \mathbf{N}^T(\nabla(\mathbf{u}\mathbf{N}))\mathrm{d}\Omega; \quad \mathbf{K}_{\pi i} \int_\Omega \mathbf{N}^T \frac{\partial}{\partial x_j}\tau_{ij}\mathrm{d}\Omega;$$

$$\mathbf{F}_i \equiv \int_\Omega \mathbf{N}^T G_x \sinh\psi(\nabla(\psi+\phi))\mathrm{d}\Omega; \quad \mathbf{K}_\mathbf{u} \equiv \int_\Omega \mathbf{N}^T u_k \frac{\partial}{\partial x_k}\left(\frac{\partial}{\partial x_j}\mathbf{N}u_j\right)\mathrm{d}\Omega;$$

$$\mathbf{f}_{\tau\mathbf{i}} \equiv \int_\Gamma \mathbf{N}^\mathbf{T}\tau_{ij}n_j\mathrm{d}\Gamma.$$

For the second step:

$$(\mathbf{B} + \Delta t^2\theta_1\theta_2\mathbf{H})\Delta\bar{\mathbf{p}} = \Delta t\left[\mathbf{G}\bar{\mathbf{U}}_\mathbf{i}^n + \theta_1\mathbf{G}\Delta\bar{\mathbf{U}}_\mathbf{i}^{\dagger} - \Delta t\theta_1\mathbf{H}\bar{\mathbf{p}}^n - \mathbf{f}_\mathbf{p}\right], \tag{22}$$

where:

$$\begin{aligned} &\mathbf{B} \equiv \int_\Omega \mathbf{N}^\mathbf{T}\frac{1}{\beta^2}\mathbf{N}\mathrm{d}\Omega; \quad \mathbf{G} \equiv \int_\Omega \frac{\partial\mathbf{N}^T}{\partial x_i}\mathbf{N}\mathrm{d}\Omega; \quad \mathbf{H} \equiv \int_\Omega \frac{\partial\mathbf{N}^\mathbf{T}}{\partial x_i}\frac{\partial N}{\partial x_i}\mathrm{d}\Omega; \\ &\mathbf{f}_\mathbf{p} \equiv \Delta t\int_\Gamma \mathbf{N}^\mathbf{T}\left[\bar{U}_i^n + \theta_1\left(\Delta\bar{\mathbf{U}}_\mathbf{i}^{\dagger} - \Delta t\frac{\partial p^{n+\theta_2}}{\partial x_i}\right)\right]n_i^T\mathrm{d}\Gamma. \end{aligned} \tag{23}$$

The third step of the algorithm becomes:

$$\Delta\bar{\mathbf{U}}_\mathbf{i} = \Delta\bar{\mathbf{U}}_\mathbf{i}^{\dagger} + \mathbf{M}^{-1}\Delta t\left[\mathbf{G}(\bar{p}^n + \theta_2\Delta\bar{\mathbf{p}}) - \frac{\Delta t}{2}\mathbf{L}\bar{\mathbf{p}}^n - \mathbf{f}_c\right], \tag{24}$$

where:

$$\mathbf{L} \equiv \int_\Omega \frac{\partial}{\partial x_i}\mathbf{N}^T u_i\frac{\partial\mathbf{N}}{\partial x_\mathrm{j}}\mathrm{d}\Omega; \quad \mathbf{f}_c \equiv \int_\Gamma (p + \theta_2\Delta p)n_i\mathrm{d}\Gamma,$$

are the matrices used.

5. Results

5.1 A benchmark problem

The first problem considered is the benchmark problem of EOF through a straight rectangular channel. The unstructured 2D mesh used for the simulations is shown in Figure 1. The mesh used is refined close to the wall to capture the rapid change in both velocity and internal potential. The length of the channel is ten times the width. The boundary conditions used are summarised below.

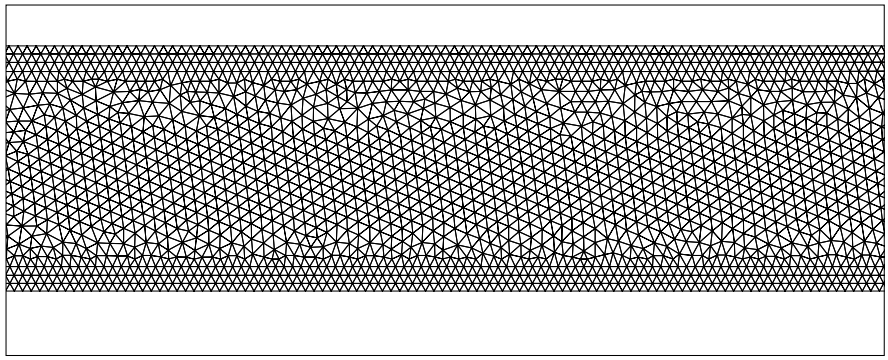

Note: A close up view of the 2D mesh used, 11,662 points and 22,094 elements

Figure 1.
EOF through a rectangular channel

On the channel walls or any solid boundary:

$$\psi = \zeta, \quad \frac{\partial \phi}{\partial y} = 0, \quad u_i = 0. \tag{25}$$

Here, ζ is the zeta potential. At the inlet, where $x = 0$:

$$\frac{\partial \psi}{\partial x} = 0, \quad \phi = \phi_1, \quad \frac{\partial u_i}{\partial x} = 0. \tag{26}$$

At the exit, where $x = L$:

$$\frac{\partial \phi}{\partial x} = 0, \quad \phi = \phi_2, \quad \frac{\partial u_i}{\partial x} = 0. \tag{27}$$

where ϕ_1 and ϕ_2 are the applied external potential values.

The numerical results obtained have been first compared with experimental data reported by Dutta *et al.* (2001) in Figure 2(a). It is, however, important to remark here that the experimental data may not be very accurate due to lack of appropriate measuring techniques to accurately determine the flow rate. Even a small disturbance

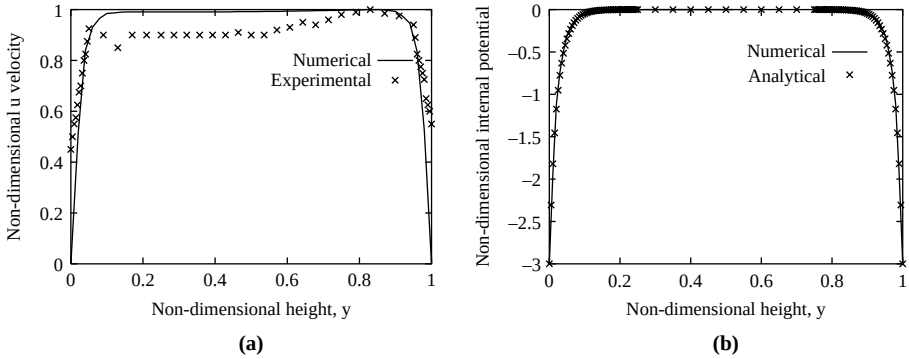

Note: Comparison of velocity profiles

Figure 2.
EOF through a rectangular channel. (a) Comparison between numerical and experimental data; (b) comparison between numerical and analytical results

such as introduction of a dye can lead to inaccuracies. This could be the reason why the agreement between the numerical and experimental data differs slightly in Figure 2(a). The parameters used to produce the results in Figure 2(a) are $ka = 40$, $\zeta = -3$, $G_x = 5.0$, $\phi_1 = 2{,}000$ and $\phi_2 = 0$.

The accuracy of the proposed method is again verified by comparing the internal potential profile with the analytical solution of Hu *et al.* (1999) as shown in Figure 2(b). The analytical solution is given as:

$$\psi = 2\ln\left[\frac{1 + \exp(-kaY^*)\tanh\left(\frac{1}{4}\zeta\right)}{1 - \exp(-kaY^*)\tanh\left(\frac{1}{4}\zeta\right)}\right], \tag{28}$$

where Y^* is the distance from the channel wall. The parameters used to produce these numerical results are: $ka = 40$, $\zeta = -3$, $\phi_1 = 2{,}000$ and $\phi_2 = 0$ and the internal potential profile was taken at a cut close to the exit of the channel. As can be seen in Figure 2(b), the analytical and numerical solutions agree excellently.

The thickness of the EDL, which depends on the bulk ionic concentration of the solution inside the channel, plays a large role in determining the shape of the flow profile within the channel. The thickness of the EDL is directly proportional to the Debye thickness, which is typically around 10 nm wide as mentioned in Patankar and Hu (1998). By changing the EDL thickness, the internal potential profile will be modified, which in turn alters the electro-osmotic velocity profile. A one dimensional analytical model of this effect was studied by Rice and Whitehead (1965). The effect of changing *ka*, which effectively alters the thickness of the EDL, is also studied in the present work. As shown in Figure 3, the gradient of the internal potential is steeper at higher *ka* values. Note that outside the EDL, the internal potential disappears – which is the reason why this potential can be neglected when considering flow on a macroscale as the EDL is so small compared to the width of the channel, and thus the electrokinetic effect has little impact on the fluid dynamics.

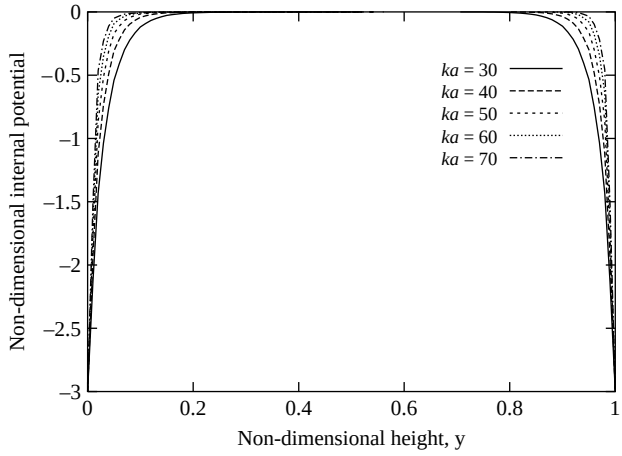

Figure 3.
EOF through a rectangular channel

Note: Effect of varying *ka* values on internal potential profiles

6. Electro-osmotic flow past a charged cylinder placed in a channel

In many practical electronic cooling situations, obstructions need to be introduced into the flow field to increase the solid surface area. One such example is the porous electro-osmotic pump. To prove the application of the proposed method to complex problems on unstructured meshes, flow though a rectangular channel with a cylindrical obstruction is studied here. The mesh used is shown in Figure 4.

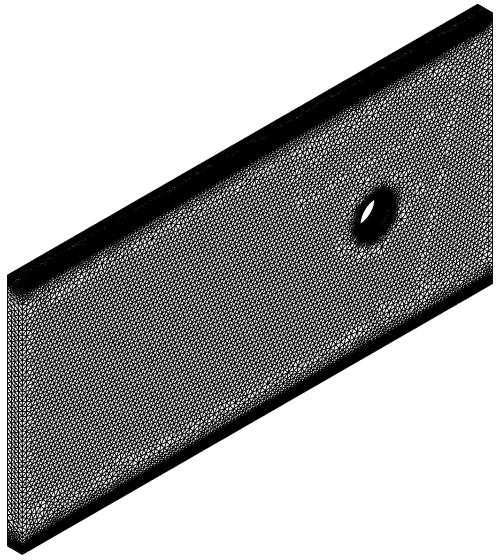

(a) Full unstructured surface mesh

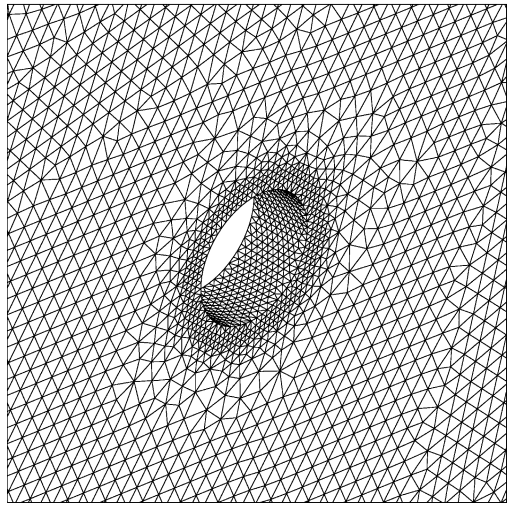

(b) Close-up view of the unstructured mesh

Note: Surface meshes

Figure 4.
Electroosmotic flow past a circular cylinder. (a) Full unstructured surface mesh; (b) close-up view of the unstructured mesh

Several unstructured meshes were tried and the mesh shown is a reasonably converged mesh. Further, refinement of the mesh give negligibly small change in solution.

In the study carried out by Ospeck and Fraden (1998), the 2D Poisson-Boltzmann equation is numerically solved. The reported study concentrates on the effect of cylinder interaction on the EDL repulsion. However, in the present paper, the effect of changing the thickness of the EDL on the internal potential and also on the velocity of the fluid inside the channel is investigated. Special attention is given to the area around the cylinder.

The non-dimensional size of the cylinder is unity. The cylinder is placed at the centre of the channel, which has a width of seven diameters. The upstream end of the channel is at a distance of three times the cylinder diameter. The downstream end of the channel is at a distance of 12 diameters from the centre of the cylinder. The cylinder is assumed to have an interaction with the electrolyte and so the top and bottom surfaces of the channel. On these solid walls no slip boundary conditions are assumed. At the inlet and exit the normal velocity gradients are assumed to be zero. Other parameters used are: $G_x = 5$, $ka = 40$, $\zeta = -3$, $\phi_1 = 2{,}000$ and $\phi_2 = 0$.

Figure 5 shows the velocity profiles in the vicinity of the cylinder. In this figure $x = 0$ is the vertical section along the centre of the cylinder. As seen the velocity profiles are distinctively different from the plug like profile obtained for channels with no obstructions. The characteristic plug like velocity profile is partly distorted in the same way as if EOF was being opposed by an adverse pressure (Dutta *et al.*, 2002). The effect of the cylinder in the path of the fluid begins to become more apparent at $x = -1$. Since, the surface of the cylinder is charged, and as a result, an EDL is developed around the cylinder, inside which ions are moving in response to the applied electric field. The fluid is seen to be pulled by either side of the cylinder in the direction of the applied electric field at this position. The horizontal velocity contours at $ka = 20$ in Figure 6 also confirms the effect of the cylinder on both upstream and downstream of the cylinder.

Figure 7(a) shows normalised u velocity profiles for different ka values at a section taken at $x = 0$ along half the width of the channel. It is in this area that the velocity of the fluid is affected predominantly by the charged cylinder. The results indicate that the higher the ka value, higher the flow rate. This is consistent with the results presented previously for a plain channel flow. The velocity profiles further down stream, at $x = 10$ are also shown in Figure 7(b) for different ka values. Again, the

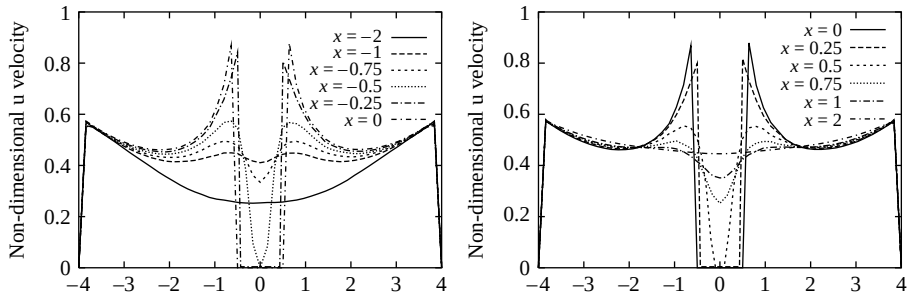

(a) Upstream of the cylinder

(b) Downstream of the cylinder

Note: u_1 velocity at different sections, $Ka = 40$

Figure 5.
EOF past a circular cylinder

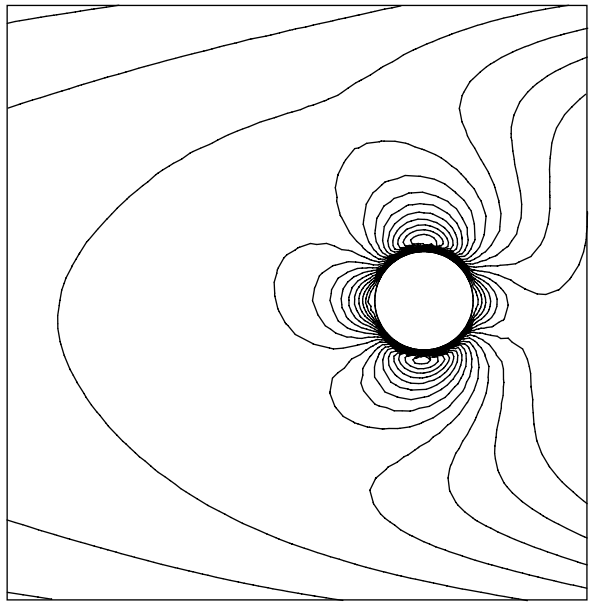

Note: Horizontal velocity distribution in the vicinity of the cylinder, ka = 20

Figure 6.
EOF past a circular cylinder

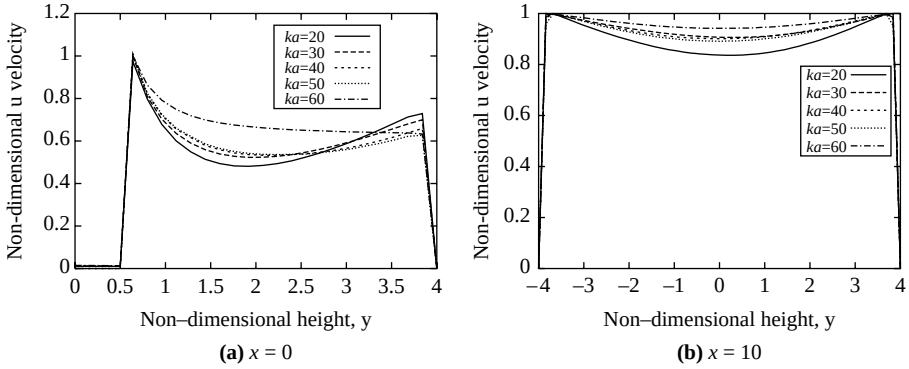

(a) x = 0 **(b)** x = 10

Note: u_1 velocity distribution for different ka values

Figure 7.
Electroosmotic flow past a circular cylinder

cylindrical obstruction clearly has some influence on the velocity profile. Unlike the plug like profiles of rectangular channel flows without obstructions, the profile obtained here has an inward curvature representing the effect of obstruction.

7. Conclusions

An explicit finite element-based solution procedure has been demonstrated for EOFs on unstructured meshes. The validity of the proposed procedure was demonstrated by comparing the results against both analytical and experimental data. The agreement between the analytical and numerical solutions was shown to be excellent.

With sufficient proof of validity for the model, a 3D problem of EOF past a circular cylinder was studied. The results shown that the velocity close to the cylinder surface is a lot larger than the velocity near the channel wall. The proposed procedure can now be confidently used in the calculation of EOF in electronic cooling devices.

References

Amon, C.H., Yao, S-C., Wu, C-F. and Hsieh, C-C. (2005), "Microelectromechanical system based evaporative thermal management of high heat flux electronics", *Transactions of the ASME*, Vol. 127, pp. 66-75.

Bianchi, F., Ferrifno, R. and Girault, H.H. (1998), "Finite element simulation of an electroosmotic – driven flow division at a T-junction of microscale dimensions", *Anal. Chem.*, Vol. 70, pp. 1870-81.

Borges, M.F., Verardi, L.L. and Machado, J.M. (2002), "Electroosmotic pumping in rectangular microchannels: a numerical treatment by the finite element method", *Applied Mathematics E-Notes*, Vol. 2, pp. 10-15.

Burgreen, D. and Nakache, F.R. (1964), "Electrokinetic flow in ultrafine capillary slits", *J. Phys. Chem.*, Vol. 68, pp. 1084-91.

Chen, X.Y., Toh, K.C., Chai, J.C. and Yang, C. (2004), "Developing pressure-driven liquid flow in microchannels under the electrokinetic effect", *Int. J. Eng. Sci.*, Vol. 42, pp. 609-22.

Dutta, P., Beskok, A. and Warburton, T.C. (2002), "Electroosmotic flow control in complex microgeometries", *Journal of Microelectromechanical Systems*, Vol. 11, pp. 36-44.

Dutta, P., Kim, M.J., Kihm, K.D. and Beskok, A. (2001), "Electroosmotic flow in a grooved microchannel configuration: a comparative study of μ-piv measurements and numerical simulations", IMECE2001/MEMS-23895.

Fu, L-M., Lin, J-Y. and Yang, R-J. (2003), "Analysis of electroosmotic flow with step change in zeta potential", *Journal of Colloid and Interface Science*, Vol. 258, pp. 266-75.

Heydari, A. and Gektin, V. (2004), "Thermal and electro-mechanical challenges in design and operation of high heat flux processors", paper presented at Inter Society Conference on Thermal Phenomena, pp. 694-6.

Hu, L., Harrison, J.D. and Masliyah, J.H. (1999), "Numerical model of electrokinetic flow for capillary electrophoresis", *Journal of Colloid and Interface Science*, Vol. 215, pp. 300-12.

Hunter, R.J. (1981), *Zeta Potential in Colloid Science, Principles and Applications*, Academic Press, London.

Intel (2006), *Intel First to Demonstrate Working 45 nm Chips*, available at: www.intel.com/pressroom/archive/releases/20060125comp.htm (accessed 2 February 2006).

Jiang, L., Mikkelsen, J., Koo, J-M., Huber, D., Yao, S., Zhang, L., Zhou, P., Maveety, J.G., Prasher, R., Santiago, J.G., Kenny, T.W. and Goodson, K.E. (2002), "Closed-loop electroosmotic microchannel cooling system for VLSI circuits", *IEEE Transactions on Components and Packaging Technologies*, Vol. 25, pp. 347-55.

Johnson, D.A., Baumann, J. and Cullimore, B. (2002), "CAD-based methods for thermal modeling of coolant loops and heat pipes", paper presented at IEEE Inter Society Conference on Thermal Phenomena, pp. 46-53.

Jon Zuo, Z., North, M.T. and Wert, K.L. (2001), "Hight heat flux heat pipe mechanism for cooling of electronics", *IEEE Transactions on Components and Packaging Technologies*, Vol. 24, pp. 220-5.

Kang, Y., Yang, C. and Huang, X. (2002), "Electroosmotic flow in a capillary annulus with high zeta potentials", *Journal of Colloid and Interface Science*, Vol. 253, pp. 285-94.

Karniadakis, G., Beskok, A. and Aluru, N. (2005), *Microflows and Nanoflows, Fundamentals and Simulation*, Springer, New York, NY.

Khuan, C.L. and Ratnam, M.M. (2006), "Design and experimental study of a cooler for a laptop computer", paper presented at Heat and Mass Transfer Conference, pp. 2376-9.

Lewis, R.W. and Garner, R.W. (1972), "A finite element solution of coupled electrokinetic and hydrodynamic flow in porous media", *International Journal for Numerical Methods in Engineering*, Vol. 5, pp. 41-55.

Lewis, R.W. and Humpheson, C. (1973), "Numerical analysis of electro-osmotic flow in soils", *Journal of the Soil Mechanics and Foundations Division*, Vol. 99, pp. 603-16.

Lewis, R.W., Nithiarasu, P. and Seetharamu, K.N. (2004), *Fundamentals of the Finite Element Method for Heat and Fluid Flow*, Wiley, New York, NY.

Löhner, R., Morgan, K. and Zienkiewicz, O.C. (1984), "The solution of non-linear hyperbolic equation systems by the finite element method", *International Journal for Numerical Methods in Fluids*, Vol. 4, pp. 1043-63.

Moore, G.E. (1965), "Cramming more components onto integrated circuits", *Electronics*, Vol. 8, pp. 114-7.

Nithiarasu, P. (2003), "An efficient artificial compressibility (AC) scheme based on the characteristic based split (CBS) method for incompressible flows", *International Journal for Numerical Methods in Engineering*, Vol. 56, pp. 1815-45.

Nithiarasu, P., Mathur, J.S., Weatherill, N.P. and Morgan, K. (2004), "Three dimensional incompressible flow calculations using the characteristic based split (CBS) scheme", *International Journal for Numerical Methods in Fluids*, Vol. 44, pp. 1207-29.

Ospeck, M. and Fraden, S. (1998), "Solving the Poisson-Boltzmann equation to obtain interaction energies between confined, like-charged cylinders", *Journal of Chemical Physics*, Vol. 109, pp. 9166-71.

Patankar, N.A. and Hu, H.H. (1998), "Numerical simulation of electroosmotic flow", *Anal. Chem.*, Vol. 70, pp. 1870-81.

Probstein, R.F. (1989), *Physicochemical Hydrodynamics*, Butterworths, Boston, MA.

Rice, C.L. and Whitehead, R. (1965), "Electrokinetic flow in a narrow cylindrical capillary", *J. Phys. Chem.*, Vol. 69, pp. 4017-24.

Sim, W.Y., Yoon, H.J., Jeong, O.C. and Yang, S.S. (2003), "A phase-change type micropump with aluminium flap valves", *J. Micromech. Microeng.*, Vol. 13, pp. 286-94.

Yang, R-J., Fu, L-M. and Hwang, C-C. (2001a), "Electroosmotic entry flow in a microchannel", *Journal of Colloid and Interface Science*, Vol. 244, pp. 173-9.

Yang, R-J., Fu, L-M. and Lin, Y-C. (2001b), "Electroosmotic flow in microchannels", *Journal of Colloid and Interface Science*, Vol. 239, pp. 98-105.

Zeng, S., Chen, C-H., Mikkelsen, J.C. Jr and Santiago, J.G. (2001), "Fabrication and characterization of electroosmotic micropumps", *Sensors and Actuators B*, Vol. 79, pp. 107-14.

Zhou, P., Hom, J., Upadhya, G., Goodson, K. and Munch, M. (2004), "Electro-kinetic microchannel cooling system for desktop computers", paper presented at IEEE SEMI-THERM Symposium.

Zienkiewicz, O.C. and Codina, R. (1995), "A general algorithm for compressible and incompressible flow – Part I: the split, characteristic-based scheme", *International Journal for Numerical Methods in Fluids*, Vol. 20, pp. 869-85.

Zienkiewicz, O.C., Taylor, R.L. and Nithiarasu, P. (2005), *The Finite Element Method for Fluid Dynamics*, Elsevier, Amsterdam.

Further reading

Chorin, A.J. (1967), "A numerical method for solving incompressible viscous flow problems", *Journal of Computational Physics*, Vol. 2, pp. 12-26.

Morgan, K., Weatherill, N.P., Hassan, O., Brookes, P.J., Said, R. and Jones, J. (1999), "A parallel framework for multidisciplinary aerospace engineering simulations using unstructured meshes", *International Journal for Numerical Methods in Fluids*, Vol. 31, pp. 159-73.

Weatherill, N.P., Hassan, O., Morgan, K., Jones, J.W. and Larwood, B. (2001), "Towards fully parallel aerospace simulations on unstructured meshes", *Engineering Computations*, Vol. 18, pp. 347-75.

Corresponding author

P. Nithiarasu can be contacted at: P.Nithiarasu@swansea.ac.uk